Title	Penetration of Alfvén waves into an upper stably-stratified layer excited by magnetoconvection in rotating spherical shells
Author(s)	Takehiro, Shin-ichi
Citation	Physics of the Earth and Planetary Interiors (2015), 241: 37-43
Issue Date	2015-04
URL	http://hdl.handle.net/2433/196750
Right	© 2015 Elsevier B.V. NOTICE: this is the author's version of a work that was accepted for publication in Physics of the Earth and Planetary Interiors. Changes resulting from the publishing process, such as peer review, editing, corrections, structural formatting, and other quality control mechanisms may not be reflected in this document. Changes may have been made to this work since it was submitted for publication. A definitive version was subsequently published in Physics of the Earth and Planetary Interiors, 241, doi:10.1016/j.pepi.2015.02.005
Type	Journal Article
Textversion	author

Penetration of Alfvén waves into an upper stably-stratified layer excited by magnetoconvection in rotating spherical shells

Shin-ichi Takehiro

Research Institute for Mathematical Sciences, Kyoto Univeristy, Sakyo-ku, Kyoto 606-8502, Japan

Abstract

The penetration of magneto-hydrodynamic (MHD) disturbances into an upper strongly stratified stable layer excited by magnetoconvection in rotating spherical shells is investigated. An analytic expression for the penetration distance is derived by considering perturbations of a stably stratified rotating MHD Boussinesq fluid in a semi-infinite region, with the rotation axis and a uniform magnetic field tilted relative to the gravity axis. Solutions for the response to MHD disturbances applied at the bottom boundary show that the disturbances propagate as Alfvén waves in the stable layer. Their propagation distance is proportional to the Alfvén wave speed and inversely proportion to both the arithmetic average of viscosity and magnetic diffusion and the total wavenumber of the disturbance. The derived expression for penetration distance is in good agreement with the numerical results for neutral convection in a rotating spherical shell with an upper stably stratified layer embedded in an axially uniform basic magnetic field.

Keywords: penetration distance, planetary fluid core, dynamo, geomagnetic secular variation

1. Introduction

Recent seismological observations have indicated the existence of a stably stratified layer below the core-mantle boundary (CMB) of the Earth (e.g. Lay and Young, 1990;

Email address: takepiro@gfd-dennou.org (Shin-ichi Takehiro)

Helffrich and Kaneshima, 2004; Tanaka, 2007; Helffrich and Kaneshima, 2010). It has also been argued that there exists a stable layer in the upper part of the fluid core of Mercury (e.g. Christensen, 2006). It was hypothesized that the composition of the stable stratification may originate from the accumulation of light elements released from the inner core and/or through barodiffusion below CMB (e.g. Gubbins and Davies, 2013; Helffrich and Kaneshima, 2013). Thermal effects have also been discussed based on the recently revised value of thermal conductivity under core conditions (e.g. Pozzo et al., 2012).

It is considered that in the unstable layer below the stably stratified layer, columnar convection elongating in the direction of the rotation axis develops due to the dominant effect of the Coriolis force. It is this that generates the intrinsic magnetic field of the planet through the dynamo process. However, since convective motion is suppressed in the stable layer, the associated generation of a magnetic field is expected to be weaker. The effects of the existence of the upper stable layer on the generated magnetic field have been investigated numerically using magneto-hydrodynamics (MHD) rotating spherical shell models; it was shown that the stable layer acts as a low-pass filter on the magnetic field, allowing small-scale magnetic field components to diffuse efficiently (e.g. Christensen, 2006; Christensen and Wicht, 2008; Nakagawa, 2011). In other models, however, filtering of the magnetic field does not occur due to strong zonal flows generated in the stable layer (Stanley and Mohammadi, 2008).

The extent of the penetration of the MHD disturbances excited by deep convective motion is one of the key issues in the MHD of stably stratified layers related to the generation of an intrinsic magnetic field through the dynamo process. Furthermore, it also plays a part in the formation of geomagnetic secular variations. Takehiro and Lister (2001) derived a theoretical expression for the penetration distance of columnar convection into the upper stable layer in non-magnetic cases δ_{NoMag}:

$$\delta_{NoMag} = \frac{2\Omega}{N} \cdot \frac{1}{K_H}, \tag{1}$$

where Ω is the angular velocity of the planet, N is the Brunt-Väisälä frequency of the stable layer, and K_H is the horizontal wavenumber of the disturbance. The scaling of the penetration depth in magnetic cases, however, is not yet known. Therefore,

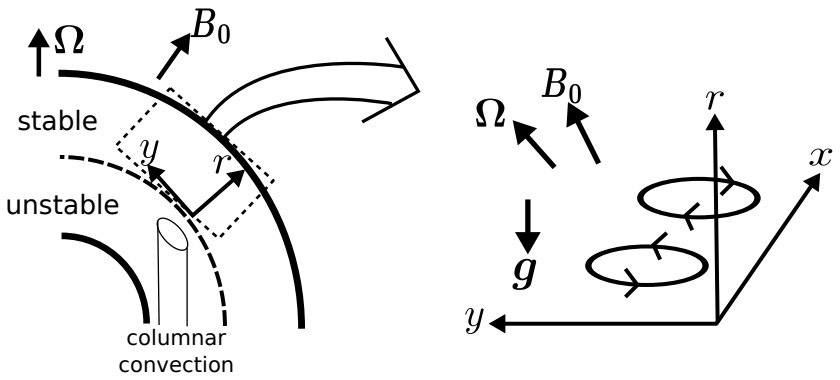

Figure 1: Schematic of the system considered.

the present paper derives a theoretical expression for the penetration depth of MHD disturbances in the outer stable layer induced by convective motions in the layer below, in the presence of the magnetic field.

2. Properties of MHD waves in a rotating strongly stratified layer

Let us consider a stably stratified rotating MHD Boussinesq fluid in the semi-infinite region $r \geq r_b$ as shown in Fig. 1, wherer $r = r_b$ is the boundary between the unstable and stable layers. The rotation axis is tilted relative to gravity (r-axis), considering the situation at mid and high latitudes of a spherical shell. In addition, a uniform magnetic field, which is also tilted relative to gravity, is imposed. The linearized equations about a state of rest are the following:

$$\frac{\partial \boldsymbol{u}}{\partial t} + 2\boldsymbol{\Omega} \times \boldsymbol{u} = -\frac{1}{\rho_0}\nabla p + \alpha g T \boldsymbol{e}_r + \frac{1}{\rho_0 \mu}(\boldsymbol{B}_0 \cdot \nabla)\boldsymbol{b} + \nu \nabla^2 \boldsymbol{u}, \tag{2}$$

$$\frac{\partial \boldsymbol{b}}{\partial t} = (\boldsymbol{B}_0 \cdot \nabla)\boldsymbol{u} + \lambda \nabla^2 \boldsymbol{b}, \tag{3}$$

$$\frac{\partial T}{\partial t} + \Gamma u_r = \kappa \nabla^2 T, \tag{4}$$

$$\nabla \cdot \boldsymbol{u} = 0, \quad \nabla \cdot \boldsymbol{b} = 0. \tag{5}$$

Here, $\boldsymbol{u}$ is the velocity, u_r is the vertical component of velocity, p is the pressure disturbance, T is the (potential) temperature, $\boldsymbol{\Omega}$ is the rotation of the system, α is the thermal expansion coefficient, g is the acceleration due to gravity, $\boldsymbol{e}_r$ is a unit vector in the

vertical (r) direction, μ is the permeability, ρ_0 is the density, $\boldsymbol{B}_0$ is the imposed basic magnetic field, $\boldsymbol{b}$ is the magnetic field disturbance, ν is the kinematic viscosity, λ is the magnetic diffusion coefficient, κ is the thermal diffusivity, and Γ is the basic vertical temperature gradient.

From the bottom boundary, i.e. $r = r_b$, a disturbance in the form of $e^{ikx+ily-i\omega t}$ is introduced, where k, l and ω are wavenumbers in the x and y directions and the frequency of the disturbance, respectively.

By operating $\boldsymbol{e}_r \cdot \nabla\times$ and $\boldsymbol{e}_r \cdot \nabla\times\nabla\times$ on (2), we can remove the pressure disturbance. Furthermore, operating $\boldsymbol{e}_r\cdot$ and $\boldsymbol{e}_r \cdot \nabla\times$ on (3) yields

$$\frac{\partial \zeta_r}{\partial t} - (2\boldsymbol{\Omega} \cdot \nabla)u_r = \frac{1}{\rho_0}(\boldsymbol{B}_0 \cdot \nabla) j_r + \nu\nabla^2\zeta_r, \tag{6}$$

$$\frac{\partial}{\partial t}\nabla^2 u_r + (2\boldsymbol{\Omega} \cdot \nabla)\zeta_r = \frac{1}{\rho_0\mu}(\boldsymbol{B}_0 \cdot \nabla)\nabla^2 b_r + \alpha g\nabla_H^2 T + \nu\nabla^2\nabla^2 u_r, \tag{7}$$

$$\frac{\partial b_r}{\partial t} = (\boldsymbol{B}_0 \cdot \nabla)u_r + \lambda\nabla^2 b_r, \tag{8}$$

$$\frac{\partial j_r}{\partial t} = \frac{1}{\mu}(\boldsymbol{B}_0 \cdot \nabla)\zeta_r + \lambda\nabla^2 j_r, \tag{9}$$

where $\zeta_r = \boldsymbol{e}_r \cdot (\nabla\times\boldsymbol{u})$ is the vertical component of vorticity, $b_r = \boldsymbol{e}_r \cdot \boldsymbol{b}$ is the vertical component of the magnetic field, $j_r = \boldsymbol{e}_r \cdot (\nabla\times\boldsymbol{b})/\mu$ is the vertical component of electric current, and $\nabla_H^2 = \nabla^2 - \partial_r\partial_r$ is the horizontal Laplacian operator.

First, let us investigate the MHD wave properties by neglecting viscosity and diffusion. Assuming that the variables are proportional to $e^{ikx+ily-i\omega t} \cdot e^{imr}$, we can obtain the following dispersion relation from Eqs. (4), (6), (7), (8), and (9):

$$\omega^4 - \left[\frac{4(\boldsymbol{\Omega} \cdot \boldsymbol{k})^2}{K^2} + \frac{N^2K_H^2}{K^2} + 2(\boldsymbol{V_A} \cdot \boldsymbol{k})^2\right]\omega^2 + (\boldsymbol{V_A} \cdot \boldsymbol{k})^2\left[(\boldsymbol{V_A} \cdot \boldsymbol{k})^2 + \frac{N^2K_H^2}{K^2}\right] = 0, \tag{10}$$

where $\boldsymbol{k} = (k, l, m)$ is the wavenumber vector, $K^2 = k^2 + l^2 + m^2$ is the square of the total wavenumber, $K_H^2 = k^2 + l^2$ is the square of the horizontal wavenumber, $N = \sqrt{\alpha g\Gamma}$ is the Brunt-Väisälä frequency, and $\boldsymbol{V_A} = \boldsymbol{B}_0/\sqrt{\rho\mu}$ is the Alfvén wave speed. Solving Eq. (10) gives

$$\omega^2 = \frac{B \pm \sqrt{B^2 - 4C}}{2},$$

$$B = \frac{4(\boldsymbol{\Omega}\cdot\boldsymbol{k})^2}{K^2} + \frac{N^2K_H^2}{K^2} + 2(\boldsymbol{V_A}\cdot\boldsymbol{k})^2,$$
$$C = (\boldsymbol{V_A}\cdot\boldsymbol{k})^2\left[(\boldsymbol{V_A}\cdot\boldsymbol{k})^2 + \frac{N^2K_H^2}{K^2}\right].$$

Further assuming that the stable stratification is sufficiently strong such that $(\boldsymbol{V_A}\cdot\boldsymbol{k})^2 \ll N^2K_H^2/K^2$, which gives $B \gg C$, then,

$$\omega^2 = \begin{cases} \dfrac{4(\boldsymbol{\Omega}\cdot\boldsymbol{k})^2}{K^2} + \dfrac{N^2K_H^2}{K^2} + 2(\boldsymbol{V_A}\cdot\boldsymbol{k})^2, \\ \dfrac{(\boldsymbol{V_A}\cdot\boldsymbol{k})^2\left[(\boldsymbol{V_A}\cdot\boldsymbol{k})^2 + \dfrac{N^2K_H^2}{K^2}\right]}{\dfrac{4(\boldsymbol{\Omega}\cdot\boldsymbol{k})^2}{K^2} + \dfrac{N^2K_H^2}{K^2} + 2(\boldsymbol{V_A}\cdot\boldsymbol{k})^2}. \end{cases} \tag{11}$$

The first mode is the inertia gravity waves modified by the imposed magnetic field (the fast mode) and the second is the slow waves (the slow mode).

The dispersion relation of the slow waves can be simplified when we assume $4(\boldsymbol{\Omega}\cdot\boldsymbol{k})^2/K^2 \ll N^2K_H^2/K^2$:

$$\omega_{slow}^2 \sim (\boldsymbol{V_A}\cdot\boldsymbol{k})^2, \qquad \omega_{slow} \sim \pm\boldsymbol{V_A}\cdot\boldsymbol{k}. \tag{12}$$

This indicates that the slow mode is the Alfvén waves (Alfvén, 1942).

When the frequency of the disturbance given at the bottom boundary ω is sufficiently small, the fast modes cannot propagate into the stable layer (evanescent). In this case their penetration distance can be estimated as

$$\frac{4(\boldsymbol{\Omega}\cdot\boldsymbol{k})^2}{K^2} + \frac{N^2K_H^2}{K^2} \sim 0, \tag{13}$$

which leads to the expression for the non-magnetic case derived by Takehiro and Lister (2001) (Eq. (1)).

On the other hand, the slow modes can propagate into the stable layer in the direction of the imposed magnetic field (wavy) however small the frequency of the disturbance is. These slow modes are the Alfvén waves whose fluid motion is restricted to the horizontal direction due to the strong stratification. These waves can be expressed by Eq. (6) with $u_r \to 0$ and Eq. (9).

3. Penetration distance of the Alfvén waves

The penetration distance of the Alfvén waves can be estimated by including the effects of viscosity and diffusion. The governing equations for the Alfvén waves are the following:

$$\frac{\partial \zeta_r}{\partial t} = \frac{1}{\rho_0}(\boldsymbol{B}_0 \cdot \nabla) j_r + \nu \nabla^2 \zeta_r, \tag{14}$$

$$\frac{\partial j_r}{\partial t} = \frac{1}{\mu}(\boldsymbol{B}_0 \cdot \nabla) \zeta_r + \lambda \nabla^2 j_r. \tag{15}$$

By taking the ξ coordinate in the direction of the imposed uniform magnetic field, the governing equations become

$$\frac{\partial \zeta_r}{\partial t} = \frac{B_0}{\rho_0}\frac{\partial j_r}{\partial \xi} + \nu \nabla^2 \zeta_r, \tag{16}$$

$$\frac{\partial j_r}{\partial t} = \frac{B_0}{\mu}\frac{\partial \zeta_r}{\partial \xi} + \lambda \nabla^2 j_r, \tag{17}$$

where $B_0 = |\boldsymbol{B}_0|$. A Fourier transformation with respect to the coordinates perpendicular to ξ,

$$\frac{\partial \zeta_r}{\partial t} = \frac{B_0}{\rho_0}\frac{\partial j_r}{\partial \xi} + \nu \left(\frac{\partial^2}{\partial \xi^2} - \tilde{K}_H^2 \right) \zeta_r, \tag{18}$$

$$\frac{\partial j_r}{\partial t} = \frac{B_0}{\mu}\frac{\partial \zeta_r}{\partial \xi} + \lambda \left(\frac{\partial^2}{\partial \xi^2} - \tilde{K}_H^2 \right) j_r, \tag{19}$$

where $\tilde{K}_H$ is the square of the total wavenumber in the plane perpendicular to ξ.

We solve these equations by assuming that the variables are proportional to $e^{i\tilde{m}\xi - i\omega t}$. The dispersion relation becomes

$$\begin{aligned} \tilde{m}^2 + \tilde{K}_H^2 \quad = \quad & \frac{1}{2\lambda\nu}\Big\{ -[-i\omega(\nu+\lambda) + V_A^2] \\ & \pm \sqrt{[-i\omega(\nu+\lambda) + V_A^2]^2 + 4\nu\lambda(\omega^2 + \tilde{K}_H^2 V_A^2)} \Big\}, \end{aligned} \tag{20}$$

where $V_A = B_0/\sqrt{\rho_0 \mu}$ is the Alfvén wave speed. When λ and ν are sufficiently small, the approximate dispersion relation is

$$\tilde{m}^2 + \tilde{K}_H^2 \sim -\frac{-i\omega(\nu+\lambda) + V_A^2}{\lambda\nu},\ \frac{\omega^2 + \tilde{K}_H^2 V_A^2}{-i\omega(\nu+\lambda) + V_A^2}.$$

The first mode is

$$\tilde{m} \sim \pm i \frac{V_A}{\sqrt{\lambda\nu}}.$$

This is the boundary mode which decays rapidly as ξ increases since λ and ν are small. On the other hand, the dispersion relation of the second mode is

$$\tilde{m} \sim \pm \left[\frac{\omega}{V_A} + i \frac{\nu + \lambda}{2} \left(\frac{\tilde{K}_H^2}{V_A} + \frac{\omega^2}{V_A^3} \right) \right],$$

which can be identified as the Alfvén waves from the real part of the wavenumber in the ξ direction, $\tilde{m}$. The imaginary part of $\tilde{m}$ expresses the extent of the attenuation due to the effects of viscosity and diffusion. Consequently, the penetration distance of the Alfvén waves $\delta_A = 1/\mathrm{Im}[\tilde{m}]$ can be written as

$$\delta_A = \frac{2}{\nu + \lambda} \left(\frac{\tilde{K}_H^2}{V_A} + \frac{\omega^2}{V_A^3} \right)^{-1} = \frac{2}{\nu + \lambda} \frac{V_A}{\tilde{K}^2}. \tag{21}$$

Here, $\tilde{K}^2 = \tilde{K}_H^2 + \tilde{m}_0^2$ is the total wavenumber of the waves and $\tilde{m}_0 = \omega / V_A$ is the wavenumber of the waves in the ξ direction. Eq. (21) means attenuation of Alfvén waves by viscosity and magnetic diffusion. Note that this expression includes neither the Brunt-Väisälä frequency of the stable layer nor the angular velocity of planetary rotation in contrast to Eq. (1) for non-magnetic cases. When we non-dimensionalize this penetration distance with the layer thickness d,

$$\frac{\delta_A}{d} = \frac{S}{\tilde{K}^2 d^2}, \quad S = \frac{2 V_A d}{\nu + \lambda}, \tag{22}$$

where S is the Lundquist number (Lundquist, 1952; Schaeffer et al., 2012). The Lundquist number is a measure for the extent of penetration of the Alfven waves, which gives the maximum wavenumber of the waves penetrating through the layer. For example, the value of the Lundquist number in the Earth's outer core is estimated as $\mathrm{O}(10^4$–$10^5)$.

4. Numerical calculations

We now compare the derived expression for the penetration distance of the Alfvén waves with the neutral MHD convection structures formed in a rotating spherical shell calculated numerically. We consider MHD Boussinesq fluid in a spherical shell with inner and outer radii of r_i and r_o, respectively, rotating with a constant angular velocity Ω. A self-gravitational force $\boldsymbol{g} = -\gamma \boldsymbol{r}$ acts on the fluid where $\boldsymbol{r}$ is the position vector

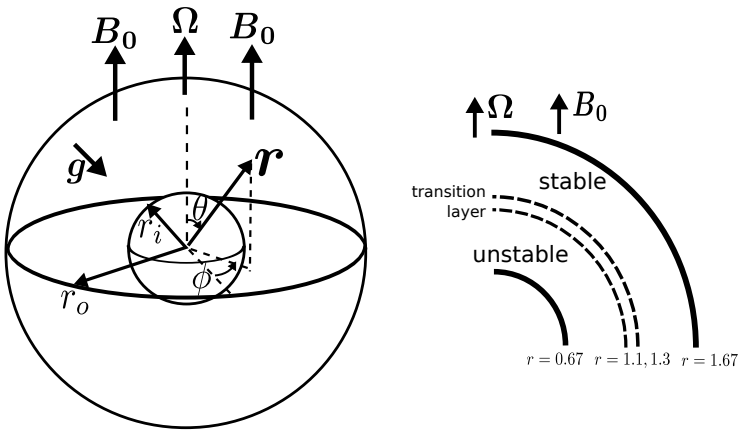

Figure 2: Schematic of the spherical shell system considered.

with respect to the center of the shell. The temperature distribution of the basic state $T_0(r)$ is the same as that used by Takehiro and Lister (2001). The inner part of the shell is unstably stratified due to uniform internal heating, while the outer part is stably stratified with a constant temperature gradient (Fig. 2).

$$\frac{dT_0}{dr} = -\frac{1}{2}(\beta r + \Gamma_0)\left[1 - \tanh\left(\frac{r - r_b}{a}\right)\right] + \Gamma_0, \tag{23}$$

where β is a parameter expressing the temperature gradient in the lower unstable layer, which is given by $\beta = Q_0/(3\rho_0 C_p \kappa)$, in which Q_0 is the uniform internal heating and C_p is the specific heat of the Boussinesq fluid. Γ_0 is the temperature gradient in the upper stable layer. $r = r_b$ is the boundary between the unstable and stable layers and a is the thickness of the transition layer. The length scale is chosen to be the thickness of the shell $d = r_o - r_i$; the time scale is the viscous diffusion time d^2/ν, the velocity scale is ν/d, the temperature scale is βd^2, and the scale of the magnetic field is the magnitude of the imposed basic magnetic field B_0. The linearized equations for the disturbances become

$$\nabla\cdot\boldsymbol{u} = 0, \quad \nabla\cdot\boldsymbol{b} = 0, \tag{24}$$

$$\frac{\partial \boldsymbol{u}}{\partial t} + \tau \boldsymbol{k}\times\boldsymbol{u} = -\nabla p + (Ra/Pr)T\boldsymbol{r} + \nabla^2\boldsymbol{u} + \Lambda\tau Pm^{-1}[(\nabla\times\boldsymbol{B}_0)\times\boldsymbol{b} + (\nabla\times\boldsymbol{b})\times\boldsymbol{B}_0] \tag{25}$$

$$\frac{\partial T}{\partial t} + u_r\frac{dT_0}{dr} = Pr^{-1}\nabla^2 T, \tag{26}$$

$$\frac{\partial \boldsymbol{b}}{\partial t} = \nabla\times(\boldsymbol{u}\times\boldsymbol{B}_0) + Pm^{-1}\nabla^2\boldsymbol{b}. \tag{27}$$

The non-dimensional parameters appearing in the equations are the square root of the Taylor number, the Rayleigh number, the Prandtl number, the magnetic Prandtl number, and the Elsasser number, which are defined as

$$\begin{aligned} \tau = \sqrt{Ta} = \frac{2\Omega d^2}{\nu}, \quad Ra = \frac{\alpha\gamma\beta d^6}{\kappa\nu}, \\ Pr = \frac{\nu}{\kappa}, \quad Pm = \frac{\nu}{\lambda}, \quad \Lambda = \frac{B_0^2}{2\Omega\rho_0\mu\lambda}. \end{aligned} \tag{28}$$

The Alfvén wave speed V_A is exppressed as $V_A = \sqrt{\Lambda\tau/Pm}$ in this system. The important non-dimensional parameter for the penetration of the Alfv́en waves, Lundquist number S, is related to these non-dimensional parameters as,

$$S = \frac{2\sqrt{Pm\cdot\Lambda\cdot\tau}}{1+Pm}. \tag{29}$$

A basic uniform magnetic field parallel to the rotation axis is imposed:

$$\boldsymbol{B}_0 = \boldsymbol{e}_r\cos\theta - \boldsymbol{e}_\theta\sin\theta, \tag{30}$$

where θ is the colatitude and $\boldsymbol{e}_r$ and $\boldsymbol{e}_\theta$ are the unit vectors in the radial and colatitudinal directions, respectively.

Fixed uniform temperature and stress-free conditions are applied to the inner and outer spheres. The magnetic field disturbance is connected with an external potential field:

$$u_r = \frac{\partial}{\partial r}\left(\frac{u_\theta}{r}\right) = \frac{\partial}{\partial r}\left(\frac{u_\phi}{r}\right) = T = 0, \quad \text{at} \quad r = r_i, r_o, \tag{31}$$

$$\boldsymbol{b} = \boldsymbol{b}_e \quad \text{at} \quad r = r_i, r_o, \tag{32}$$

where (u_r, u_θ, u_ϕ) are the radial, colatitudinal, and azimuthal components of velocity, respectively, and $\boldsymbol{b}_e = \nabla^2 W$ is the external potential field.

We intorduce toroidal and poloidal potentials to express solenoidal velocity and magnetic fields (e.g. Glatzmaier, 1984). The governing equations and boundary conditions for these potentials and temperature are expanded with spherical harmonic functions and Chebyshev polynomials in the horizontal and radial directions, respectively.

Furthermore, by assuming that the variables are proportional to $\exp(\sigma t)$, the system becomes a linear eigenvalue problem for each azimuthal wavenumber with respect to the eigenvalue σ (growth rate). For a given set of parameters, the growth rate σ can be obtained by solving the linear eigenvalue problem. Through an iterative procedure with respect to Ra, a neutral solution where the real part of σ vanishes is sought.

For the numerical calculations, the total wavenumber minus the azimuthal wavenumber of the spherical harmonics is truncated at 30, while the Chebyshev polynomials are calculated up to the 32nd order. Moreover, in order to reduce computational time and resources, the poloidal velocity field, toroidal magnetic field, and temperature field are assumed to be equatorially symmetric, while the toroidal velocity field and poloidal magnetic field are assumed to be equatorially antisymmetric.

We fix the values of the radius ratio to 0.4 ($r_i = 0.6667, r_i = 1.6667$). We also consider the case with $\tau = 10^5$, $Pr = 1$, $r_b = 1.2$, and $a = 0.05$. The value of the temperature gradient Γ_0 is set to 10^3. The magnetic Prandtl number Pm and the Elsasser number Λ are varied by setting $Pm = 0.2, 1, 5$ and $\Lambda = 5 \times 10^{-2}, 0.1, 0.2, 0.5, 1, 2, 5$. The azimuthal wavenumber is varied from 16 to 25.

Figure 3 compares the meridional structures of the azimuthal velocity field, the radial components of vorticity, and the electric currents of the obtained neutral convection modes for various values of the Elsasser number Λ. When the basic magnetic field is weak ($\Lambda = 0.2$, $S = 141.4$), all the variables are trapped below the stable layer. This is consistent with the penetration distances for non-magnetic cases Eq. (1) proposed by Takehiro and Lister (2001), which was $O(10^{-2})$. However, it is found that the MHD disturbances gradually penetrate the stable layer as Λ, and S, is increased and the basic magnetic field is strengthened. Note that the control parameter for penetration of the Alfvén waves is not Λ but S. In the case of Figure 3, when Λ is increased, the Alfvén wave speed becomes larger but the diffusion parameters are fixed, then the Lundquist number S is increased, resulting deep penetration of the MHD disturbances. Also note that even the values of the Lundquist number are the same, the structures of MHD disturbances are not necessarily the same, since the wavenumber $\tilde{m} \sim \omega/V_A$ may be different.

Figure 4 compares the structures of the azimuthal velocity field, the radial com-

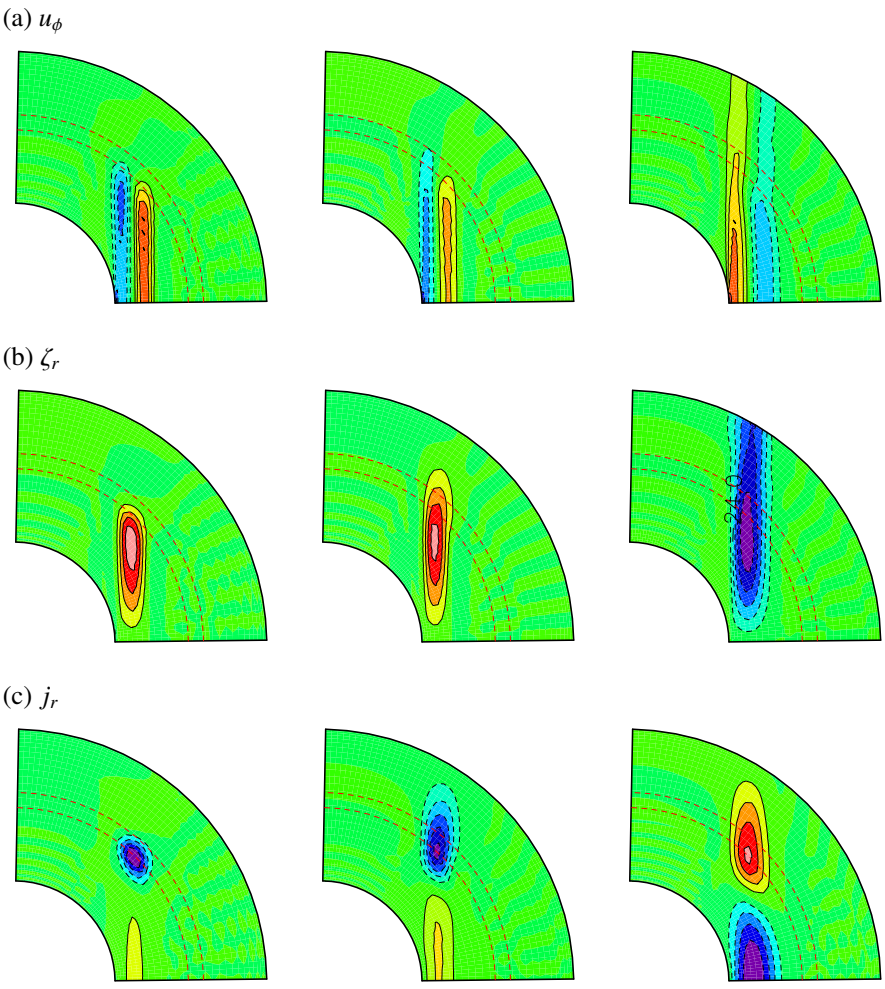

Figure 3: Comparison of the meridional structures of neutral convection. $\tau = 10^5$, $Pm = 1$, and the azimuthal wavenumber is 22. From left to right, $\Lambda = 0.2, 1, 5$ ($S = 141.4, 316.2, 707.1$), respectively. (a) the azimuthal velocity, u_ϕ, (b) radial vorticity ζ_r, (c) radial components of the electric current j_r. The red broken lines indicate the transition layer ($r = 1.15$ and 1.25).

ponent of vorticity, and the electric current for the obtained neutral convection modes for various values of the Elsasser number Λ. The comparison is made on the cylindrical surface at $s = 0.9$, where s is the cylinder's radial coordinate. When the basic magnetic field is weak ($\Lambda = 0.2$, $S = 141.4$), the wavefronts are tilted from the axial direction (the direction of the imposed basic magnetic field) although the amplitudes of the variables are small in the stable layer compared with those in the inner unstable layer, resulting in a large $\tilde{m}_0$. In contrast, when the basic magnetic field is strengthened, the wavefronts of the MHD disturbances become parallel to the axial direction, meaning that $\tilde{m}_0$ decreases. This tendency can be understood by considering the dispersion relation of the Alfvén waves, $\omega = V_A \tilde{m}_0$. When the basic magnetic field is strengthened while the frequency of the convective motion in the lower layer remains relatively constant, the Alfvén speed V_A increases and $\tilde{m}_0$ decreases as a result.

In order to compare the numerical results with the theoretical estimates obtained previously, the penetration distance and wavenumber in the axial direction of the neutral modes are evaluated as follows. Taking the z coordinate in the axial direction, we consider a variable $f(z)$ that can be expressed as

$$f(z) = Ae^{imz - z/\delta} = |A|e^{i(mz+\alpha)-z/\delta},$$

where m is the wavenumber in the z direction, δ is the characteristic penetration distance, and α is the phase at $z = 0$. By sampling the data at two observational points $z = z_1$ and z_2, we obtain

$$\delta = -\frac{z_1 - z_2}{\log(|f(z_1)|/|f(z_2)|)}, \quad m = \frac{\tan^{-1}(s_1) - \tan^{-1}(s_2)}{z_1 - z_2}. \tag{33}$$

Here, $s_i = \tan(mz_i + \alpha)$. For comparison of numerical results and theoretical estimations, we choose the observational points so that $z_1 = z_b + 0.1$ and $z_2 = z_b + 0.2$ on the cylindrical surface where the amplitude of ζ_r becomes maximum, where $z = z_b$ is the location of the bottom of the stable layer $r = r_b$. Figures 5 and 6 compare the values of δ and m obtained numerically with those estimated theoretically. We evaluate the square of the total wave number perpendicular to the axial direction $\tilde{K}_H$ as $\tilde{K}_H^2 = (m_\phi/s_{obs})^2 + (\pi/0.15)^2$. Here, m_ϕ is the azimuthal wavenumber and s_{obs} is the cylindrical radial coordinate of the observational points. $\pi/0.15$ is the value of the

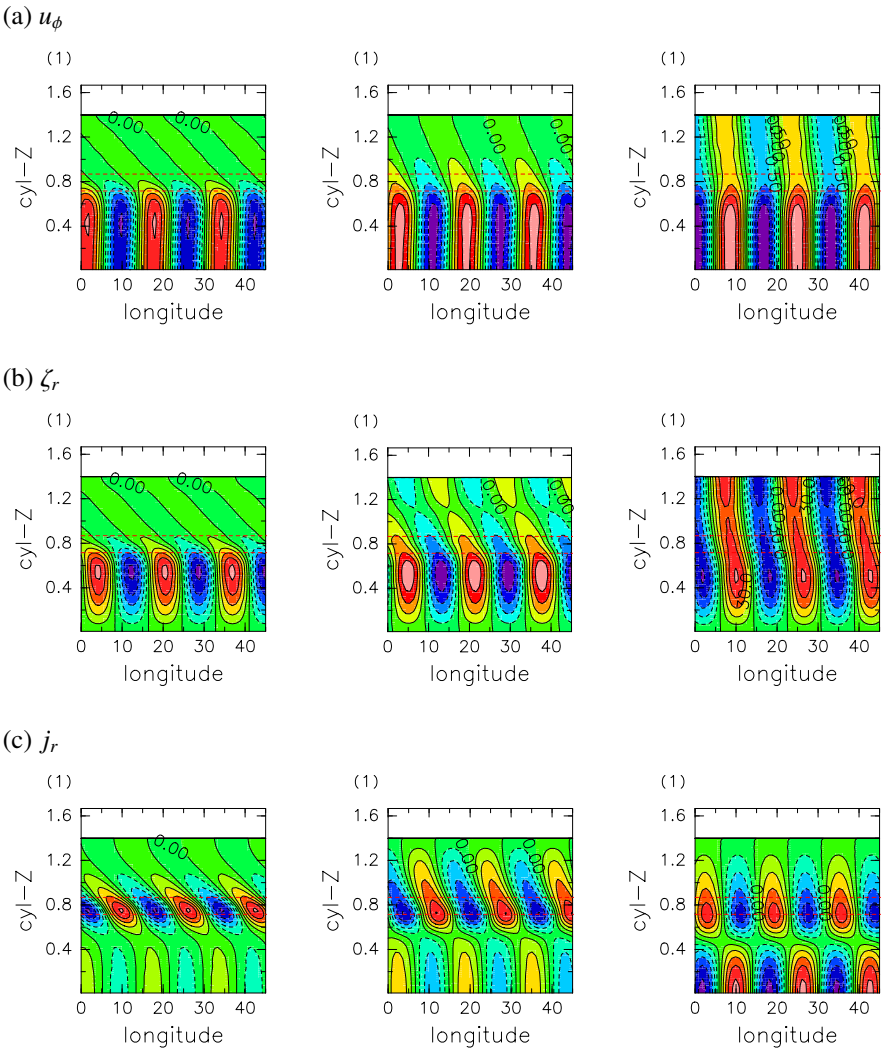

Figure 4: Comparison of the cylindrical structures of azimuthal velocity components at the surface of a cylinder of radius $s = 0.9$. $\tau = 10^5$, $Pm = 1$, and the azimuthal wavenumber is 22. From left to right, $\Lambda = 0.2, 1, 5$ ($S = 141.4, 316.2, 707.1$), respectively. (a) the azimuthal velocity, u_ϕ, (b) radial vorticity ζ_r, (c) radial components of the electric current j_r. The red broken lines indicate the transition layer ($z = \pm 0.72$ and ± 0.87).

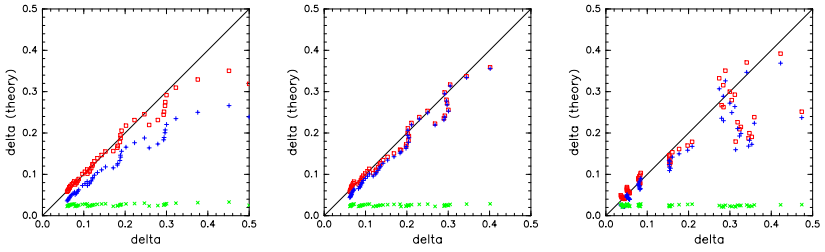

Figure 5: Comparison of propagation distance. $\tau = 10^5$. From left to right, $Pm = 0.2$, 1 and 5, respectively. The abscissa is the propagation distance of the Alfvén waves measured from the distribution of ζ_r, which is obtained through numerical calculations of neutral thermal convection. The ordinate is the theoretical estimate of the propagation distance, which is indicated by blue crosses (21). Red squares denote the propagation distance obtained by solving (20) without the approximation. Green crosses indicate the penetration distance without a magnetic field derived by Takehiro and Lister (2001) (Eq. 1).

wavenumber in the cylinder's radial direction, which is roughly measured from the meridional cross-sections.

In the case with $Pm = 1$ (Fig. 5 center), the blue crosses are located along the line of $y = x$, indicating good agreement between the theoretical estimations and the numerical results for the penetration distance. In contrast, the distribution of the green crosses shows that the penetration distance in the non-magnetic case (1) cannot explain the numerical results. In the case with $Pm = 0.2$ (Fig.5 left), the theoretical penetration distance is in good agreement with, albeit a little smaller than, the numerical results. In the case with $Pm = 5$ (Fig.5 right), the theoretical penetration distance again matches the numerical results when $\delta \leq 0.2$; however, when $\delta \geq 0.3$, the agreement is to a lesser extent.

The center panel of Fig. 6 compares the theoretically estimated and numerical values of the wavenumber m for the case of $Pm = 1$. The blue crosses are located along the line of $y = x$, indicating good agreement between the theoretical estimations and the numerical results for the axial wavenumber. In the case with $Pm = 0.2$ (Fig. 6 left), the results for the theoretical axial wavenumber are in good agreement, although the theoretical values are systematically slightly smaller than the numerical values. In the case with $Pm = 5$ (Fig. 6 right), the theoretical axial wavenumber distance is in good agreement with the numerical values except when $m \geq 15$.

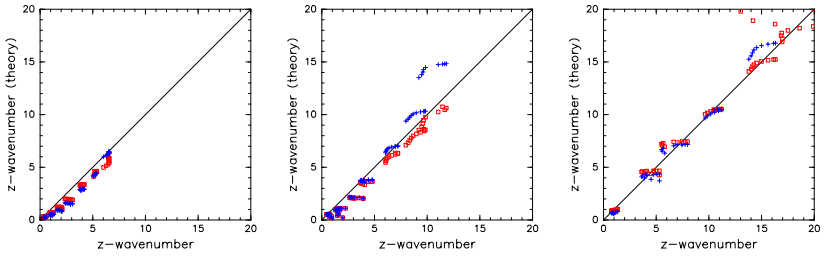

Figure 6: Comparison of the axial wavenumbers. $\tau = 10^5$. From left to right, $Pm = 0.2$, 1 and 5, respectively. The abscissa is the wavenumber of the Alfvén waves measured from the distribution of u_ϕ, which is obtained through numerical calculations of neutral thermal convection. The ordinate is the theoretical estimate of the axial wavenumber. Blue crosses indicate the theoretical estimate using ω/V_A. Red squares denote the propagation distance obtained by solving (20) without the approximation.

5. Concluding remarks

We investigated the influence of deep convection on the MHD fluid motion in the upper stably stratified layer considering the effects of the magnetic field. We found that the Alfvén waves are able to propagate into the stable layer however strong the stratification is. We proposed an analytical expression for the penetration distance of the Alfvén waves, which is proportional to the Alfvén wave speed and inversely proportional to both the arithmetic average of viscosity and magnetic diffusion and the total wavenumber of the waves. The neutral modes of MHD thermal convection in a rotating spherical shell with an upper stably stratified layer and the axially uniform magnetic field were reproduced numerically. It was observed that the MHD disturbances trapped below the stable layer gradually penetrate into the stable layer as the imposed magnetic field is strengthened. The penetration distance and axial wavenumber of the numerical solutions are in good agreement with the theoretical analytic expressions proposed in this study.

Note that the Alfvén waves propagate in the direction of the basic magnetic field. When the basic magnetic field in the stable layer is in the horizontal direction (a toroidal field in a spherical shell geometry), the Alfvén waves cannot propagate through the stable layer. Therefore, the horizontal (toroidal) basic magnetic field inhibits the penetration of MHD disturbances into the stable layer. On the other hand, when the basic

magnetic field is in the vertical direction (a poloidal field in a spherical shell geometry), the Alfvén waves are able to penetrate the stable layer efficiently.

Also note that the rotating spherical shell model discussed in section 4 is a special case where the basic magnetic field is imposed in the direction of the rotating axis in order to illustrate the penetration of Alfvén waves clearly. In general cases where the basic magnetic field does not align exactly with the rotation axis, the theoretical results derived in this paper suggests that penetration occurs in the direction of the basic magnetic field rather than the rotating axis.

From a geophysical perspective an interesting variable is the radial component of the magnetic field, which can be observed at a planet's surface. In the simplified plane layer model used for theoretical investigation of wave properties, MHD disturbances in the strongly stratified layer are not expected to have a radial component of the magnetic field, because they are the Alfvén waves with inhibited vertical fluid motion. However, in the stable layer of a spherical shell, the radial component of the magnetic field can be induced through advection of a basic magnetic field in the horizontal direction in the induction terms:

$$\frac{\partial b_r}{\partial t} \sim -\frac{u_\phi}{r\sin\theta}\frac{\partial B_{0r}}{\partial \phi} - \frac{u_\theta}{r}\frac{\partial B_{0r}}{\partial \theta}. \tag{34}$$

The results in the present study suggest that the Alfvén waves may be excited and penetrate the upper stable layer in the numerical calculations of MHD dynamos in rotating spherical shells performed in previous works (e.g. Christensen, 2006; Christensen and Wicht, 2008; Nakagawa, 2011). It was found in these studies that the stable layer filters out and weakens the magnetic field generated in the convective lower layer by observing the radial component of the magnetic field. However, the toroidal components of velocity and the magnetic field, which are the main constituents of the Alfvén waves, may not be attenuated by the stable layer.

Finally, we discuss the possibility of the penetration of MHD disturbances into the upper stable layer of the fluid cores of the Earth and Mercury. If we assume $\bar{B}_r \sim 10^{-3}$T in the stable layer of the Earth's outer core, the Alfvén wave speed becomes $V_A = \bar{B}_r/\sqrt{\rho\mu} \sim 10^{-2}$ m/s. Then the Lundquist number becomes $S \sim 10^3$, when we use the values of the stable layer thickness thickness and the magnetic diffusivity as $O(10^2)$km

and $\eta = 1\mathrm{m}^2/\mathrm{s}$, respectively, and the viscosity is neglected. From the condition $\delta_A/d = S/(K^2d^2) > 1$, the maximum wavenumber K_M of the waves penetrating through the stable layer is estimated as $O(10^{-3})$ m^{-1}. On the other hand, considering the westward drift component of the geomagnetic field (e.g. Bullard et al., 1950; Yukutake, 1962; Finlay and Jackson, 2003), the total horizontal wavenumber is assumed to be 10, and the frequency to be $\omega \sim 10^{-9}$ s^{-1}, which makes the total wavenumber $K \sim 10^{-6}$ m^{-1}. This is much smaller than K_M estimated above (the propagation distance $\delta_A \sim 10^9$ m, which is much larger than the expected thickness of the stable layer). Therefore, some components of geomagnetic secular variation may be explained by the Alfvén waves propagating through the stable layer excited by the deep convection.

In contrast, since observed Mercury's magnetic field is quite weak, the Lundquist number is small compared with the Earth. When we assume the magnetic field strength is about O(10^3–10^4) nT based on the surface value of 500nT, the Alfvén wave speed is estimated as O(10^{-5}–10^{-6}) m/s. Although the thickness of the stratified layer is uncertain, we assume that it is comparable to the that of the fluid core thickness of O(10^6)m (Christensen and Wicht, 2008). Then the value of the Lundquist number becomes O(1–10), suggesting that only the global MHD disturbances are possible to penetrate through the stratified layer.

Acknowledgements

The numerical calculations were performed on the computer systems of the Research Institute for Mathematical Sciences of Kyoto University. The library for spectral transforms 'ISPACK'(Ishioka, 2013) and its Fortran90 wrapper library 'SPMODEL library'(Takehiro et al., 2013) were used for the numerical calculations. The products of the Dennou-Ruby project (`http://www.gfd-dennou.org/arch/ruby/`) were used to draw the figures.

References

Alfvén, H., 1942. Existence of electromagnetic-hydrodynamic waves. Nature, 150, 405–406.

Bullard, E.C., Freedman, C., Gellman, H., Nixon, J., 1950. The westward drift of the Earth's magnetic field. Phil. Trans. R. Soc. Lond. A 243, 67–92.

Christensen, U. R., 2006. A deep dynamo generating Mercury's magnetic field. Nature 444, 1056–1058.

Christensen, U. R., and J. Wicht, 2008. Models of magnetic field generation partly stable planetary cores: Applications to Mercury and Saturn. Icarus 196, 16–34.

Finlay, C.C., Jackson, A., 2003. Equatorially dominated magnetic field change at the surface of Earth's core. Science 300, 2084–2086.

Gubbins, D., and Davies, C. J., 2013. The stratified layer at the core-mantle boundary caused by barodiffusion of oxygen, sulphur and silicon. Phys. Earth Planet. Inter. 225, 21–28.

Glatzmaier, G. A., 1984. Numerical simulations of stellar convective dynamos I – The model and method. J. Comp. Phys. 55, 461–484.

Helffrich, G. and Kaneshima, S., 2004. Seismological constraints on core composition from Fe-O-S liquid immiscibility. Science 306, 2239–2242.

Helffrich, G. and Kaneshima, S., 2010. Outer-core compositional stratification from observed core wave speed profiles. Nature 468, 808–810.

Helffrich, G., and Kaneshima, S., 2013. Causes and consequences of outer core stratification. Phys. Earth Planet. Inter. 223, 2–7.

Ishioka, K., 2013. ispack-1.0.2. GFD Dennou Club, `http://www.gfd-dennou.org/library/ispack/`.

Lay, T. and Young, C.J., 1990. The stably-stratified outermost core revisited. Geophys. Res. Lett. 17, 2001–2004.

Lundquist, S., 1952. Studies in magneto-hydrodynamics. Arkiv for Fysik 5, 297–347.

Pozzo, M., Davies, C., Gubbins, D., and Alfe, D., 2012. Thermal and electrical conductivity of iron at Earth's core conditions. Nature 485, 355–358.

Stanley, S., and A. Mohammadi, 2008. Effects of an outer thin stably stratified layer on planetary dynamos. Phys. Earth Planet. Inter. 168, 179–190.

Nakagawa, T., 2011. Effect of a stably stratified layer near the outer boundary in numerical simulations of a magnetohydrodynamic dynamo in a rotating spherical shell and its implications for Earth's core. Phys. Earth Planet. Inter. 187, 342–352.

Schaeffer, N., Jault, D., Cardin, P., Drouard, M., 2012. On the reflection of Alfvén waves and its implication for Earth's core modelling. Geophys. J. Int., 191, 508–516.

Takehiro, S, and J. R. Lister, 2001. Peneration of columnar convection in an outer stably stratified layer in rapidly rotating spherical fluid shells. Earth Planet. Sci. Lett. 187, 357–366.

Takehiro, S., Sasaki, Y. Ishioka, K., Odaka, M. Takahashi, Y.O, Nakajima, K., Ishiwatari, M., Hayashi, Y.-Y. and SPMODEL Development Group, 2013. Hierachical Spectral Models for GFD (SPMODEL). GFD Dennou Club, `http://www.gfd-dennou.org/library/spmodel`

Tanaka, S., 2007. Possibility of a low P-wave velocity layer in the outermost core from global SmKS waveforms. Earth Planet. Sci. Lett. 259, 486–499.

Yukutake, T., 1962. The westward drift of the magnetic field of the Earth. Bull. Earth. Res. Inst. 40, 1–65.